An Imaging Device that Uses the Wavelet Transformation as the Image Reconstruction Algorithm

John H. Letcher

Department of Mathematical and Computer Sciences, University of Tulsa, Tulsa, Oklahoma 74104
and
Cyrix Corporation, Richardson, Texas 75081

ABSTRACT

Many imaging devices have been constructed that use fourier transform techniques for image reconstruction as well as for image analysis. The basis functions in the fourier transform space are sinusoids. These are not localized. Therefore it should not be expected that highly localized behavior of a signal be characterized well using functions distributed evenly throughout the interval of the integral transform. Also, the phase cancellations of a conventional impulse signal are not handled well by fourier techniques. On the other hand, the basis functions of the wavelet transformation are highly localized, i.e., these exhibit compact support, yet are orthonormal. The multispectral decomposition algorithm of the wavelet transformation is used to analyze the signal returning from the reflections of a single ultrasonic transducer with a focused beam and operated in the focal zone. The choice of frequency depends upon the mutually antagonistic factors of penetration (αf^{-2}) and resolution (αf). The signal sent into the sample should not be the impulse response signal used in conventional devices; rather, it should be a time-reversed replica of a single or a linear combination of the most highly localized basis function wavelets. The returning signal is a sequence of translates of the wavelets plus perhaps some lower-resolution wavelets. The translations are proportional to the time of flight of the signal. The wavelet transformation is superb at discriminating the population of each of these translates which is identically the A-scan signal. The transmitted signal, which is a time-reversed single wavelet or a linear combination of wavelets, is not easy to produce. Inexpensive ultrasound transducers have resonances which make it difficult to produce any desired wave form. Wavelet shape is far from arbitrary. Precise wave shaping is performed by measuring the impulse response function of the transducer; then, the desired wave shape is convolved with the inverse of the measured impulse response function of the transducer. This produces the signal to be presented to the pulse generation circuit. Care is taken to damp the impulse response so that there are no zeros. The received signal is sampled at an even rate which is carefully chosen to match the time delay of one wavelet translate to the next. B-scan, C-scan, and volume imaging are easily accomplished using a sequence of A-scan data, all by conventional techniques. A single A-scan requires less than 2 ms to perform and reconstruct with a high-speed arithmetic unit which was designed in conjunction with this work and is now commercially available.

I. INTRODUCTION

Conventional ultrasound imaging devices fall into a number of categories. Some of these are used to study systems containing boundaries where the acoustic impedance Z of a material ($Z \equiv \rho v$, where ρ is the density and v is the velocity of sound in the material) [1] differs greatly from one material to the next. In such a system, the reflections are strong and multiple reflections are common. In systems such as living tissue the difference of impedance from one material to the next (such as from muscle to fat) generate weak reflections. This article deals only with the latter such system.

An A-scan is a map of the boundaries that is generated by directing a thin ray of sound into a material and recording a digitized time series of the reflections of the sound. The usual case is to subject a piezoelectric crystal to a single large voltage spike (~200 volts for a duration of tens of nanoseconds). The crystal deforms along the electric field and because of the contraction and dilation of the crystal produces sound at one end of the crystal. The other end is held firmly by a sound-absorbing material such as a plastic with tungsten particles imbedded in the plastic.

Although the impressed voltage is quite sharp and well defined, the crystal is not particularly cooperative in tracking the applied voltage. What is seen are multiple oscillations that usually dampen out in four or five cycles at a frequency determined by the physical characteristics of that particular crystal (crystals are commercially available throughout the 1–50 MHz range that will probably be employed for medical imaging purposes). The crystal is normally supplied with a lens to produce a focused ray of sound with a sharp pattern only a few degrees wide. The characteristics of the lens determines the focal length F. The transmitting crystal may be and usually will be used as the receiving transducer. The useful range of the fine focus is from about 0.66 F to 2.0 F.

A variety of schemes exist to move the beam of sound between a sequence of A-scans, so as to produce a B-scan, a two-dimensional map of what the A-scan performs in one dimension. The C-scan is a map in a plane orthogonal to the A-scans and is generated by straightforward computer software techniques. Any scheme that is employed to extend conventional ultrasound may be employed with the device reported herein. Therefore the use of mechanical means to move the transducer or the use of phased arrays of transducers are generally used; these will not be discussed here. Rather, we will concentrate on the development of a new technique for obtaining a superior A-scan. Extension to two or three dimensions should be straightforward and contains nothing else which is particularly novel.

Received 3 December 1991; revised manuscript received 8 January 1992

International Journal of Imaging Systems and Technology, Vol. 4, 98–108 (1992)

CCC 0899-9457/92/020098-11$04.00

Conventional devices either view the raw signal or employ techniques based on the Fourier transform to yield an image. One fourier technique uses the calculation of a correlation function which tries to decompose the received into a sequence of the blurred transmitted signal which is sent into the material. Phase cancellation of one reflection with another makes this signal extremely difficult to analyze by fourier techniques. A map of the raw signal of a perfectly sharp boundary produces an imprecise blur at least to the extent that the transmitted signal is smeared in time. Since it is not reasonable to ask for crystals with all but perfect impulse response functions, we must live with the wiggles in the signal. We must therefore change the mathematics that is employed to discriminate one reflection from the next rather than relying entirely on forcing the crystal to do what it does not want to do.

Fourier techniques all employ basis functions that are not localized at all in the transform space. This suggests that if we were to use a set of basis functions that are highly localized, we might obtain superior results. This is the case when we employ the wavelet transformation.

II. INTEGRAL TRANSFORMS

The set of equations

$$g(a) = \int_{I_1} K_1(x, a)h(x)\,dx\,, \tag{1}$$

$$h(x) = \int_{I_2} K_2(x, a)g(a)\,da \tag{2}$$

defines an integral transform pair. The function $g(a)$ is called the transform of $h(x)$, and the variables x and a are called conjugate variables.

To define a specific (named) transform, the two Kernel functions $K_1(x, a)$ and $K_2(x, a)$ must be defined. Similarly, the interval over which each integration is carried out must be specified. Finally, something must be stated with regard to the properties of the functions g and h for the transform and its inverse to exist.

The fourier transform is defined by

$$K_1 \equiv (2\pi)^{-1/2}\exp(-ixa)\,, \tag{3}$$

$$K_2 \equiv (2\pi)^{-1/2}\exp(+ixa)\,, \tag{4}$$

$$I_1 = [-\infty, +\infty]\,, \tag{5}$$

and

$$I_2 = [-\infty, +\infty]\,. \tag{6}$$

It is sufficient that

$$\int_{I_1} |h(x)|^2 dx < \infty \tag{7}$$

and

$$\int_{I_2} |g(a)|^2 da < \infty \tag{8}$$

for the transform and its inverse to exist.

Please notice that the set of basis functions $\{\exp(inx)\}$, $n = 0, \pm 1, \ldots$ are orthogonal. Also note that both intervals are infinite in extent. For use on a digital computer, it would be preferable to use finite intervals (i.e., basis functions of finite or even compact support).

We can convert the infinite fourier transformation to the finite discrete fourier transformation. However, in the process, we must now assume that the function we wish to transform is periodic on the interval of the discrete transform. This has unfortunate consequences.

It would be preferable to use an integral transform that has the following properties:

1. The basis functions are nonzero only over a finite interval (compact support).
2. The basis functions are orthonormal (orthogonal and normalized).
3. The decomposition/reconstruction (transform/inverse transform) algorithms should be efficient and if recursive, rapidly converging.

III. WAVELET TRANSFORMATIONS

The wavelet transform extends the notion of an integral transform and adds another level of spectral resolution. Rather than the transform being a function of one conjugate variable, it is to have a pair of conjugate variables, thus

$$g(a,b) = \frac{1}{|a|^{1/2}} \int w\left(\frac{x-b}{a}\right) h(x)\,dx\,, \tag{9}$$

$$h(x) = \frac{1}{2\pi C_w} \iint w\left(\frac{x-b}{a}\right) |a|^{-1/2} g(a,b)\,\frac{da\,db}{a^2}\,, \tag{10}$$

where

$$C_w = \int d\zeta\,|\hat{w}(\zeta)|^2\,\zeta^{-1} \tag{11}$$

and

$$\hat{w}(\zeta) = (2\pi)^{-1/2} \int e^{-ix\zeta} w(x)\,dx\,. \tag{12}$$

The parameters a and b can be chosen to vary continuously ($a, b \in \mathbf{R}$ with $a \neq 0$) or in a discrete way [$a = a_0^m$, $b = nb_0a_0^m$, with $m, n \in \mathbf{Z}$ (i.e., m and n are integers) and with $a_0 > 1$, $b_0 > 1$, invariant]. We choose to use the latter.

We intend to construct our wavelet transformation by using a "scaling function" which is defined in terms of a dilation equation which employs a set of expansion coefficients $\{C_k\}$. We will then build (using the set of expansion coefficients $\{C_k\}$) the wavelets out of a linear combination of these scaling functions. The wavelets that we construct form a complete orthonormal basis. Please understand that although the algorithms are given below to calculate these wavelets, *it is not necessary to do so* to calculate the transforms of experimental data and then to reconstruct.

IV. SCALING FUNCTIONS

Consider a scaling function $\phi(x)$ that has the following properties: Given the dilation equation in terms of a set of coefficients $\{C_k\}$, $k = 0, 1, \ldots, M-1$, then

$$\phi(x) = \sum_{k=0}^{M-1} C_k \phi(2x-k) . \tag{13}$$

We wish to require that

$$\int \phi(x)\, dx = 1 \tag{14}$$

and that the coefficients are such that $C_k = 0$ for $k < 0$ and for $k \geq M$.

If we multiply Eq. (13) by 2 and integrate over x, it can be shown that

$$\sum_{k=0}^{M-1} C_k = 2 . \tag{15}$$

We would like to require that for some p,

$$\sum_{k=0}^{M-1} C_k (-1)^k k^m = 0 \quad \text{for } m = 0, 1, \ldots, p-1 . \tag{16}$$

Also, we would like to require that

$$\sum_{k=0}^{M-1} C_k C_{k-2m} = 2\delta_{0m} . \tag{17}$$

The function $\phi(x)$ can be evaluated by starting with a beginning function, $\phi_0(x)$ and iterating

$$\phi_j(x) = \sum_{k=0}^{M-1} C_k \phi_{j-1}(2x-k) , \quad j = 1, \ldots . \tag{18}$$

This will converge to the desired scaling function $\phi(x)$ at all diadic points $x = k/2^j$.

For the box function (the Haar wavelet) $\phi_0(x) = 1$, $0 < x < 1$, 0 otherwise, and there are two nonzero coefficients, $C_0 = 1$, $C_1 = 1$, and $p = 1$. The convergence is immediate and $\phi = \phi_0$.

For the Daubechies scaling function $D_4(x) \equiv \phi(x)$, we use $\phi_0(x) = 1$ when $0 < x < 1$, 0 otherwise. Also, we use only four nonzero coefficients, C_k. That is, $M = 4$, and

$$C_0 = (1+\sqrt{3})/4, \quad C_1 = (3+\sqrt{3})/4 ,$$
$$C_2 = (3-\sqrt{3})/4 , \quad C_3 = (1-\sqrt{3})/4 .$$

For the D_4 scaling function, $p = 2$.

Note that if there are recursion coefficients $C_0, \ldots, C_{K-1}$, then ϕ is zero outside the interval $[0, K]$. From continuity considerations, we have $\phi(0) = \phi(K) = 0$. [However, with the box function, with $K = 1$, both $\phi(0)$ and $\phi(1)$ may not be zero.]

V. PROPERTIES OF THE SCALING FUNCTION

From Eq. (13) we have

$$\phi(x-n) = \sum_{k=0}^{M-1} C_k \phi(2x-2n-k) . \tag{19}$$

The scaling function is orthogonal to all of its translates, i.e.,

$$I_n \equiv \int \phi(x)\phi(x-n)\, dx = 0 \quad \text{for } n \neq 0 , \quad n \in Z. \tag{20}$$

Note that when $|n| \geq M-1$, the integrand is identically zero.

Using the substitution $s = x - n$, $ds = dx$, we have

$$I_n \equiv \int \phi(s+n)\, \phi(x)\, ds$$

Therefore $I_n = I_{-n}$.

The scaling function is *not* orthogonal to its dilations. In fact,

$$\int \phi(2^{j_1}x)\, \phi(2^{j_2}x)\, dx = 2^{-j} \tag{21}$$

when j is the larger of j_1 and j_2.

For the D_4 scaling function Eq. (15) states that

$$C_0 + C_1 + C_2 + C_3 = 2 . \tag{22}$$

From Eq. (16) for the D_4 wavelet

$$C_0 - C_1 + C_2 - C_3 = 0 \tag{23}$$

and

$$-C_1 + 2C_2 - 3C_3 = 0 . \tag{24}$$

From Eq. (17) for the D_4 wavelet ($m = 0$)

$$C_0^2 + C_1^2 + C_2^2 + C_3^2 = 2 \tag{25}$$

and for cases of $m = \pm 1$,

$$C_0 C_2 + C_1 C_3 = 0 . \tag{26}$$

It is interesting to note that

$$C_0^2 + C_1^2 = C_0 + C_1 , \tag{27}$$

which is a property that is useful in the reconstruction algorithm. Therefore, from Eq. (22) and Eq. (25),

$$C_2^2 + C_3^2 = C_2 + C_3 . \tag{28}$$

VI. THE WAVELETS

Remembering that the scaling function ϕ has M nonzero coefficients, C_k, we may now express a wavelet $W(x)$ as

$$W(x) = \sum_{k=2-M}^{1} (-1)^{k+1} C_{1-k} \phi(2x-k) . \tag{29}$$

Using the substitution $n = 1 - k$, i.e., $k = 1 - n$

$$W^M(x) \equiv W(x) = \sum_{n=0}^{M-1} (-1)^n C_n \phi(2x-1+n) . \tag{30}$$

Also,

$$W(2^j x - k) = \sum_{n=0}^{M-1} (-1)^n C_n \phi(2^{j+1}x - 1 + n - 2k) . \tag{31}$$

From Eq. (16) using $m = 0$ and Eq. (14)

$$\int W(x)\,dx = \sum_{k=2-M}^{1} (-1)^{k+1} C_{1-k} \int \phi(2x-k)\,dx\,. \tag{32}$$

Using the substitution, $s = 2x - k$, $ds = 2dx$,

$$\int W(x)\,dx = \sum_{k=2-M}^{1} (-1)^{k+1} C_{1-k} \int \phi(s)\,\frac{ds}{2}$$

$$= \sum_{k=2-M}^{1} (-1)^{k+1}\,\frac{C_{1-k}}{2}\,. \tag{33}$$

Now if we employ the substitution $k = 1 - n$, it is not difficult to show that

$$\int W(x)\,dx = \tfrac{1}{2} \sum_{n=0}^{M-1} (-1)^n C_n = 0\,. \tag{34}$$

It can also be seen that

$$\int W(nx-k)\,dx = \int W(s)\,ds/n = 0/n = 0 \tag{35}$$

by using $s = nx - k$, $ds = n\,dx$, for all n and k, $n \neq 0$.

$$\int |W(x)|^2\,dx = \sum_{k_1=2-M}^{1} \sum_{k_2=2-M}^{1} (-1)^{k_1+k_2+2} C_{1-k_1} C_{1-k_2}$$

$$\times \int \phi(2x-k_1)\,\phi(2x-k_2)\,. \tag{36}$$

Using $n_1 = 1 - k_1$, $n_2 = 1 - k_2$, i.e., $k_1 = 1 - n_1$ and $k_2 = 1 - n_2$, we have

$$\int |W(x)|^2\,dx = \sum_{n_1=0}^{M-1} \sum_{n_2=0}^{M-1} (-1)^{n_1+n_2} C_{n_1} C_{n_2}$$

$$\times \int \phi(s)\,\phi(s-n_1+n_2)\,\frac{ds}{2}\,. \tag{37}$$

For the D_4 wavelet, $\int \phi(s)\,\phi(s-n_1+n_2)\,ds = 0$ unless $n_1 = n_2$. Thus,

$$\int |W(x)|^2\,dx = \sum_{n_1=0}^{M-1} \sum_{n_2=0}^{M-1} (-1)^{2n_1} C_{n_1} C_{n_2} = \sum_{n=0}^{M-1} C_n^2 = 1\,. \tag{38}$$

One more property worth mentioning is that

$$W(2^j x - n) = -W(n + 1 - 2^j x)\,. \tag{39}$$

We may now define

$$W_{jk}^M(x) \equiv W_{jk}(x) \equiv 2^{j/2} W(k - 2^j x)\,. \tag{40}$$

Out of these we may expand a function $f(x)$ in terms of multiresolution expansion coefficients b_{jk}, thus

$$f(x) = f^{\phi} + \sum_{j,k} b_{jk} 2^{-j/2} W_{jk}(x)\,, \quad j = 0, \ldots; \quad k = 0, \ldots, 2^j\,. \tag{41}$$

Note that b_{jk} carries information about f near $x = 2^j$ and near $x = 2^{-j}k$. The sum on k is the detail at the scaling level, 2^j.

In summary, as has been shown, these functions, our wavelets, are orthogonal to their own dilations and their own translations. That is,

$$\int W(x)\,W(2^j x - k)\,dx = \delta_{j0}\delta_{jk}\,, \quad j, k \in Z\,. \tag{42}$$

There are *two* indices, one for translation, k, and one for dilation (or compression), j.

Plots of the scaling function and the lowest sequency Haar wavelets are given in Fig. 1. Figure 2 gives a plot of the D_4 scaling function and Fig. 3 gives the lowest sequency wavelet. Higher-order wavelets are formed mathematically in a manner identical to the Haar wavelets.

Other wavelets may be formed by a linear combination of

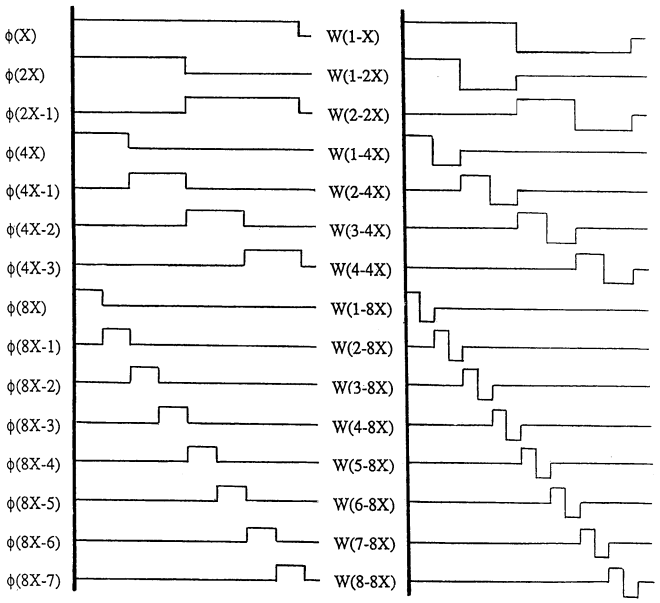

Figure 1. The Haar wavelet.

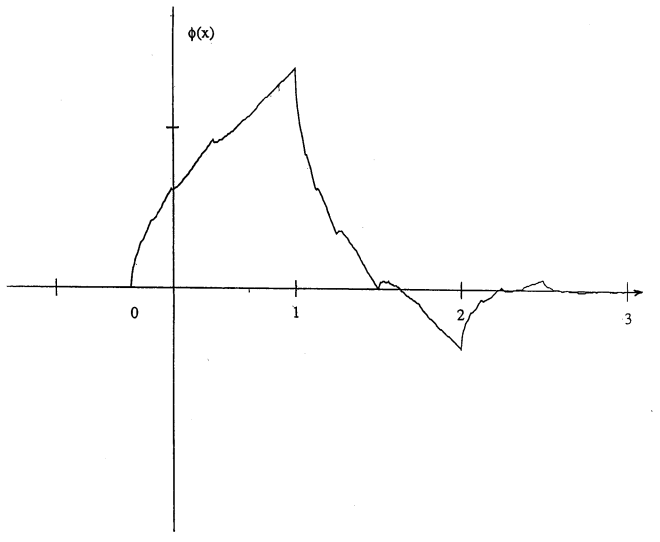

Figure 2. The D_4 scaling function.

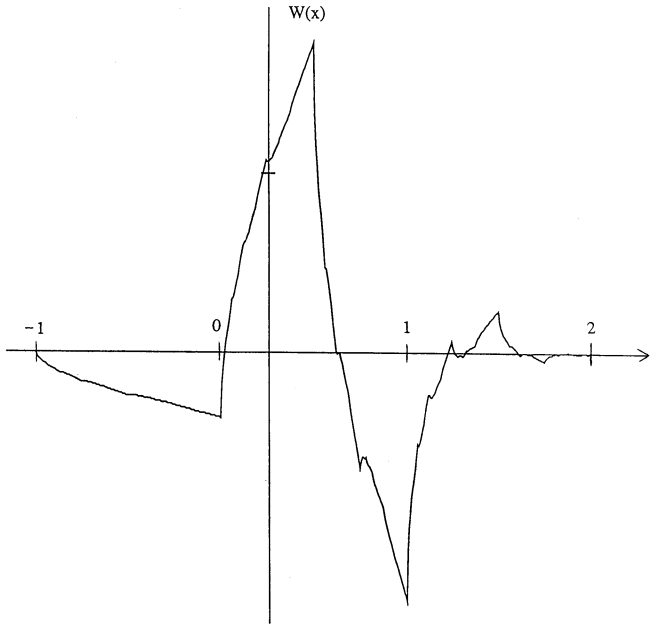

Figure 3. The D_4 wavelet.

wavelets. That is,

$$L^M = L^M_{jk}(x) = \sum_{n=1}^{m} d_n(j,k) \quad W^M_{jk}(x) . \tag{43}$$

In order to achieve the wavelet properties listed in this section, it is found that the choice of the sets $\{C_k\}$ is far from arbitrary. Only special combinations of precise values are allowed. Otherwise one or several of the desired wavelet properties will be lost. For ease of understanding, the specific wavelet forms that are to be used in the imaging device will be defined as Letcher Wavelets, or $\mathbf{L^M}$, with the wavelets in the form generated by Eqs. (18), (30), (40), and, ultimately, (43) with $M = 2, 4, 6, \ldots$.

VII. SEQUENCY [2]

Frequency is a parameter that distinguishes the individual functions of sets of sinusoids $\{\cos 2\pi ft\}$ or $\{\sin 2\pi ft\}$. Its usual physical interpretation is "number of cycles per unit of time." The generalized frequency may be interpreted as "average number of zero crossing per unit of time divided by 2" or as "average number of sign changes per unit of time divided by 2." The normalized, generalized frequency is interpreted as "average number of zero crossings per time interval of duration 1 divided by 2." The generalized frequency has the dimension $[s^{-1}]$. The definition of the generalized frequency has been chosen so that it coincides with that of frequency, if applied to sine and cosine functions. The zero crossings of sine and cosine functions are equally spaced but the definition of the generalized frequency makes it applicable to functions whose zero crossings are not equally spaced and which need not even be periodic.

It is useful to introduce the new term "sequency" for the generalized frequency. The measure of sequency is "average number of zero crossings per second divided by 2." When the term sequency is applied to wavelets, it refers to the average number of zero crossings per unit time divided by 2, considering only that time when the wavelet is nonzero.

VIII. FUNCTION DECOMPOSITION

We are given a vector of N $(=2^J)$ data values $[f_1, \ldots, f_N] \equiv \mathbf{F}$, representing the function f, where the time spacing of the data values are evenly spaced on a unit interval. The goal is to split this vector $\mathbf{F}$ into its components at different scales, indexed by j. At each new level the mesh width is cut in half and the number of wavelet coefficients is doubled. The composition is

$$f = f^{\phi} + f^{(0)} + f^{(1)} + \cdots + f^{(J-1)} + f^{\mathrm{err}} , \tag{44}$$

$$f^{(j)} = \sum_{k=1}^{2^j} b_{jk} 2^{-j/2} W_{jk}(x) = \sum_{k=1}^{2^j} b_{jk} W(k - 2^j x) , \tag{45}$$

and

$$f^{\phi}(x) = b_{\phi}\phi(1-x) , \tag{46}$$

$$f^{\mathrm{err}} = \sum_{j=J}^{\infty} \sum_{k=1}^{2^j} b_{jk} W(k - 2^j x) . \tag{47}$$

Note that $f^{\mathrm{err}} = 0$ at $x =$ any of the sampled points. The detail $f^{(j)}$ is a combination of 2^j wavelets at scale 2^{-j}. f^{ϕ} is a multiple of the scaling function ϕ.

The wavelet transformation will accept a vector of N data values, $\mathbf{F}$, and produce a vector of N values, $\mathbf{B}$ plus a vector of length $N-1$, $\mathbf{A}$. The inverse transformation will accept a vector of N values, $\mathbf{B}$, and produce a vector N values, $\mathbf{F}$, plus a vector of length $N-1$, $\mathbf{A}$. The first element of $\mathbf{A}$ is identical to the first element of $\mathbf{B}$; therefore, it is redundant. Please note that both the transform and its inverse will produce the detail vector $\mathbf{A}$.

IX. THE WAVELET TRANSFORM ALGORITHMS

The algorithms, that perform the forward and inverse transformations have been described before, almost. Strang [3] states that we can define four sets of matrices ${}^n\mathbf{E}$, ${}^n\mathbf{H}$, ${}^n\mathbf{E}^*$, and ${}^n\mathbf{H}^*$ such that

$$({}^n\mathbf{E})_{ij} \equiv C_{2i-j}/2 , \tag{48}$$

$$({}^n\mathbf{E}^*)_{ij} \equiv C_{2i-j} , \tag{49}$$

$$({}^n\mathbf{H})_{ij} \equiv (-1)^{j+1} C_{j+1-2i}/2 , \tag{50}$$

$$({}^n\mathbf{H}^*)_{ij} \equiv (-1)^{j+1} C_{j+1-2i} . \tag{51}$$

The preceding superscript n denotes the size or dimensionality of the matrix. That is to say that ${}^n\mathbf{E}$ is a 1 by $2l$ matrix where $2l = 2^n$, i.e., ${}^3\mathbf{E}$ is 4 by 8. For the D_4 wavelet the matrices $\mathbf{E}$ and $\mathbf{H}$ are shown in Fig. 4. As the dimensionality is increased, it is done by repeating, thereby increasing the pattern to the right and down. Notice the two orphan terms in row 1 of $\mathbf{E}$ and row l of $\mathbf{H}$.

The matrices ${}^n\mathbf{E}^*$ and ${}^n\mathbf{H}^*$ are the transposes of ${}^n\mathbf{E}$ and ${}^n\mathbf{H}$ except that the factor of $\frac{1}{2}$ is not present.

Because of the properties we have imposed on the set $\{C_n\}$ given in Eqs. (15), (16), and (17), it can be shown that for each n,

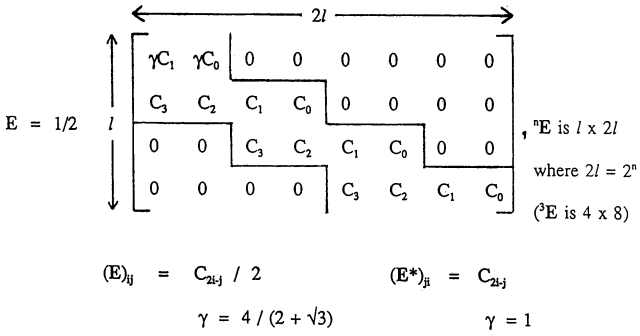

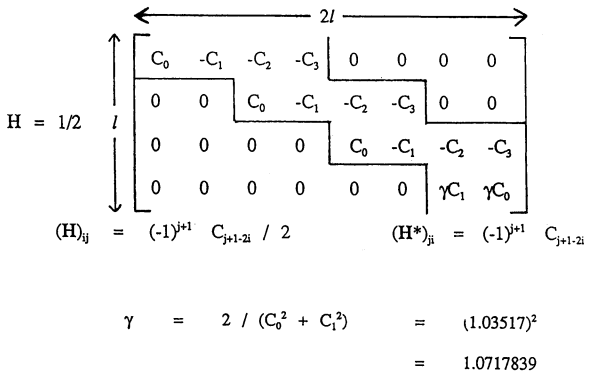

Figure 4. The matrices **E** and **H** for the D_4 wavelet.

$$ {}^n\mathbf{E}{}^n\mathbf{E}^* = {}^n\mathbf{H}{}^n\mathbf{H}^* = \mathbf{1} \quad \text{which is } l \times l\,, \tag{52} $$

$$ {}^n\mathbf{E}^*{}^n\mathbf{E}^* + {}^n\mathbf{H}^*{}^n\mathbf{H} = \mathbf{1}\,, \quad \text{which is } 2l \times 2l\,, \tag{53} $$

$$ {}^n\mathbf{H}{}^n\mathbf{E}^* = {}^n\mathbf{E}{}^n\mathbf{H}^* = \mathbf{0}\,, \quad \text{which is } l \times l\,, \tag{54} $$

that is, if we introduce, unlike Strang, a multiplicative factor γ to the orphan terms in each matrix. The symbol **1** represents a matrix of ones on the diagonal and zeros elsewhere, and **0** is a matrix of all zeros. Here, for the above relations to hold,

$$ \gamma = 2/(C_0^2 + C_1^2) = 1.071\,783\,9\,. \tag{55} $$

These matrices are shown diagrammatically in Fig. 4.

The forward wavelet transformation algorithm is shown schematically in Fig. 5. Starting with a linear array **F** which is $l \times 1$ (and is defined to be $\mathbf{A}^n$, $n = 2^l$), then two arrays, $\mathbf{A}^{n-1}$ and $\mathbf{B}^{n-1}$, can be calculated by the process

$$ \mathbf{A}^{n-1} := {}^n\mathbf{E}\mathbf{A}^n \tag{56} $$

and

$$ \mathbf{B}^{n-1} := {}^n\mathbf{H}\mathbf{A}^n\,. \tag{57} $$

This process is repeated until $n - 1 = 1$. Then the arrays ${}^n\mathbf{A}$ and ${}^n\mathbf{B}^*$ are accumulated into single arrays **A** and **B**. This is shown schematically in Fig. 5.

Notice that in each step, the computational burden is cut in half. This decimation accounts for the $O(N \log_2 N)$ behavior of the algorithm.

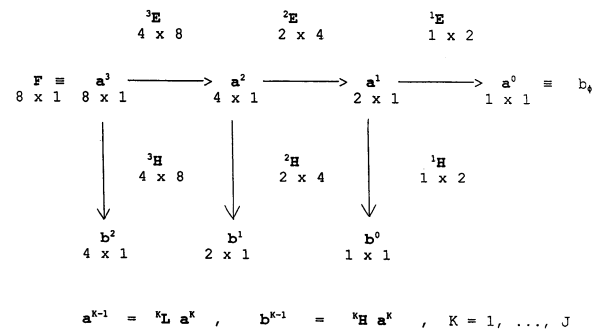

Figure 5. The wavelet transform algorithm.

The inverse wavelet transform uses the matrices $\mathbf{E}^*$ and $\mathbf{H}^*$ as shown in Fig. 6. The single **B** array is used selectively to calculate a new set of $\mathbf{A}^n$ arrays. Finally, the array **F** is obtained.

$$ \mathbf{A}^{n+1} := {}^n\mathbf{E}^*\mathbf{A}^n + {}^n\mathbf{H}^*\mathbf{B}^n\,, \tag{58} $$

$$ \mathbf{F} = \mathbf{A}^k\,, \tag{59} $$

where k is the final value of n. This algorithm is shown diagrammatically in Fig. 6.

We can visualize the action of both the forward and inverse transformation as shown in Fig. 7. The large arrow pointing to the right indicates that the **F** is transformed into arrays **A** and **B**. The inverse transformation uses only the **B** array to calculate *both* the **F** and **A** arrays. The **A** array is automatically calculated in either form of the transformation. The functions listed immediately to the left of the **B** array in Fig. 7 are the basis functions which correspond to the coefficients in the **B** array.

The question might arise, "Would it be possible to force the calculation to go faster if the **A** array were not calculated?" The answer is no. The values of the **A** array (as they are calculated) are needed in each stage of the calculation of the **B** array (forward) and the **F** array (inverse).

The algorithm is basically the pyramid algorithm of Mallat [3]. This is an algorithm that is extremely efficient and is R ($N \log_2 N$). The D_4 wavelet transformation software has been written as well as fourier transformation software to take full advantage of the architecture of the Cyrix Corporation EMC87 memory-mapped high-speed coprocessor to a 80386 computer. All of the software described in this article is commercially available from Cyrix Corporation.

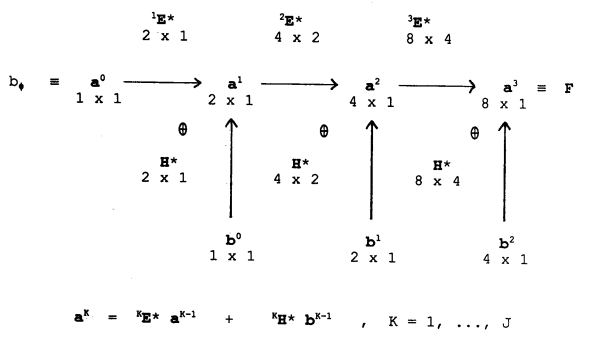

Figure 6. The inverse wavelet transform algorithm.

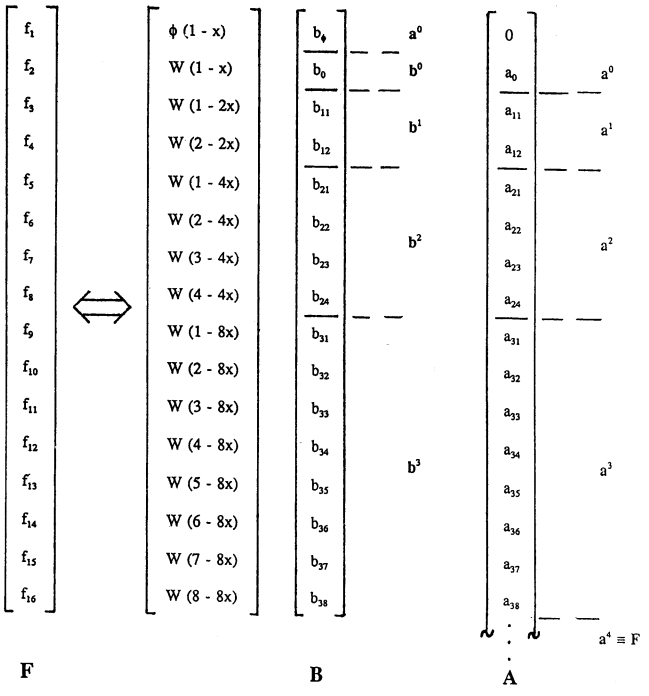

Figure 7. The wavelet transform (for $N = 16$, $J = 4$).

X. INTERPRETATION OF THE A AND B ARRAYS

We are given a set of data values F_i, $i = 1, \ldots, N$. F_i is the sampled value of F at the value of x_i. The x_i values are evenly spaced on the unit interval, i.e., $x_{i+1} - x_i = 1/N$.

In any transformation of this type, we wish to chose a set of N functions $\{\psi_j\}$ which exhibit orthogonality and normalization. We wish to find a set of coefficients so that the function F is expressed as a linear combination of the basis functions, that is,

$$F_i = F(x_i) = (F)_i = \sum_{k=1}^{N} b_k \psi_k(x_i), \quad i = 1, \ldots, N. \tag{60}$$

For the wavelet transformation, $\psi_1 = \phi(1-x)$, $\psi_2 = W(1-x)$, $\psi_3 = W(1-2x)$, $\psi_4 = W(2-2x)$, etc. The array **B** is calculated so that $(\mathbf{B})_k \equiv b_k$. There are N coefficients as **F** is real.

The discrete complex fourier transformation is defined in an identical way except that the basis functions are defined as

$$\begin{aligned} \psi_k &= (2\pi)^{-1/2} \cos(2\pi knx), \\ \psi_{k+1} &= (2\pi)^{-1/2} \sin(2\pi knx). \end{aligned} \tag{61}$$

The basis functions are sinusoids with sine–cosine pairs each at different frequencies. Notice that for an N point Fourier transform, $2N$ basis functions are required because the function to be transformed is complex and it is sampled to yield N real and N imaginary point values.

If we view the wavelet basis functions each as a single-cycle sinusoid that is nonzero only over one cycle, then our approximate wavelets could be.

$$\begin{aligned} \psi_1 &= \phi(1-x) = \text{a constant}, \quad \psi_2 = W(1-x) \\ &= \sin[2\pi(1-x)], \quad \text{etc.} \end{aligned}$$

Notice that there are only ν different sequencies ($N \equiv 2^\nu$), $N/2$ of the highest sequency, $N/4$ of the next lower, etc. The $N/2$ basis functions of the highest sequency are such that the number of the ordered set is displaced one from the other by exactly one cycle.

The interpretation of the B array is straightforward: N functions have been chosen as a set of basis functions of a space into which F shall be projected. The elements of the array B are the fraction of the function F represented by each basis function. By limiting the number of basis functions to a small (finite) number, we limit the class of functions that can be represented exactly. In the fourier transform, the basis functions that are not used are all sinusoids of frequency greater than the maximum listed in Eq. (60) by letting $n = N - 1$. This gives rise to aliasing and the Gibbs phenomenon if the sampled signal contains frequencies greater than one half of the sampling frequency (the Nyquist frequency). In the case of the wavelet transformation, those basis functions which are not used are those of higher sequency than those employed, i.e., of higher-order dilations.

The **A** array can be broken into a sequence of subarrays of progressively larger size. The first array has a length of one, the second has a length of two, the next four, etc. Each of these subarrays can be interpreted as being what the **F** array would become if all higher-order sequencies (corresponding to the sequencies of the respective **B** elements) were removed. That is, the highest-order subarray of **A** is the array **F** with the highest sequency removed, the next subarray is the array **F** with the highest two sequencies removed, etc. If we view this as a form of low-pass filter, a sequence of successive applications of low-pass filters is identically the **A** array.

XI. THE SAMPLING INTERVAL

In the act of calculating the **A** and **B** arrays, the wavelets, W_k and the scaling function ϕ are never evaluated. Yet, when one asks the question, if we were to calculate the set of points g_i, $i = 1, \ldots, n$ from the equation

$$g_i = g(x_i) = b_\phi \phi(1 - x_i) + \sum_{j=0}^{J-1} \sum_{k=1}^{2^j} b_{jk} W(k - 2^j x_i) \tag{62}$$

where

$$x_i = (i/N) - KX, \quad i = 1, \ldots, N \quad \text{and} \quad 0 \le KX \le 1/N$$

and

$$(\mathbf{B})_1 = b_\phi$$

and

$$(\mathbf{B})_m = b_{jk}, \quad m = 2^j + k - 1,$$

then how precise is the representation? To answer this question, consider the function Error, the error of representation, which is expressed as

$$\text{Error} \equiv \tfrac{1}{2} \sum_{i=1}^{N} (f_i - g_i)^2. \tag{63}$$

This function is intrinsically positive and will equal zero only when all g_i is equal to the corresponding f_i.

Using the eight-point forward transformation software discussed above, the value of Error was calculated as a function KX. Note that $1/8 = 0.125$, the fraction of the unit interval occupied by each data point. For the Haar wavelet, Error is identically zero for all values of $KX > 0.0$ and $KX < 0.125$. This means that if the eight values of F are defined on the unit interval, and evenly spaced in the interval, it does not matter where in the 0.125 portion of the unit interval that you place the first point. However, with the D_4 wavelet, it is found that the value of Error is surprisingly sensitive to the value of KX. Table I is the set of calculated values of the error of representability, Error as a function of the position in the interval by taking samples as shown in Fig. (8). Therefore, in the case of the D_4 wavelet, the error is sensitive to any offset (translation) of the sampling grid within the unit interval. A value of 0.167 E + 01 was obtained by spreading the sample over the entire interval (with a spacing of 1/7 with a point at each end point).

XII. THE ULTRASOUND A-SCAN; A REVIEW OF THE PHYSICS

Consider a plane wave of sound in a material with acoustical impedance $Z_i \equiv \rho_i v_i$, and absorption coefficient μ_i, where ρ_i is the density and v_i is the velocity of sound in the material i. The intensity I of the sound at a distance x within the material is given by

$$I = I_0 e^{-\mu_i x} . \tag{64}$$

Scattering of sound out of the beam is considered to be absorption. If the medium is homogeneous, no reflections are generated traversing the medium. However, if a boundary is encountered between media of two different impedances, then some of the sound will be reflected directly back (R) and the rest will be transmitted through the boundaries (T), i.e., $T = I - R$ [1].

$$R = I \frac{Z_2 - Z_1}{Z_2 + Z_1} . \tag{65}$$

In water, $v = 1.483 \times 10^5$ cm/s, $\rho = 1$ g/cm^3, $Z_1 = 1.483 \times 10^5$ g/cm^2 s. In muscle, $v = 1.55 \times 10^5$ cm/s, $\rho = 1.08$ g/cm^3. Therefore, $Z_2 = 1.68 \times 10^5$ g/cm^2 s.

Table I.

KX	Error	KX	Error
0.001	0.146E + 1	0.080	0.492E-2
0.010	0.812E + 0	0.086	0.859E-3
0.020	0.509E + 0	0.087	0.781E-3
0.030	0.283E + 0	0.088	0.803E-3
0.040	0.202E + 0	0.090	0.125E-2
0.050	0.103E + 0	0.100	0.162E-1
0.060	0.402E-1	0.110	0.503E-1
0.070	0.228E-1	0.120	0.101E + 0
		0.124	0.127E + 0

$$R/I = (Z_2 - Z_1)/(Z_2 + Z_1) = 0.12/3.08 = 0.039 \tag{66}$$

and

$$T/I = 2Z_1/(Z_2 + Z_1) = 2.96/3.08 = 0.961 , \tag{67}$$

where $Z_2 < Z_1$, the magnitude of the reflected wave is the same as when $Z_1 < Z_2$. However, the phase of the reflected signal is reversed. To a first approximation, multiple back reflections occur with probability $\sim[(Z_2 - Z_1)/(Z_2 + Z_1)]^3$; therefore these may be ignored. To a first approximation, the devices received signal is a sequence of primary reflections.

XIII. THE IMAGING DEVICE

Consider a directed beam of sound the magnitude of the intensity of which is a time-reversed wavelet of sequency j. At first glance, what one would expect to find is a sequence of wavelets which are translates of each other, one for each reflection boundary. The time for receipt is the time of flight of the sound. Some slight wavelet broadening may be expected; however, we assume that the broadening will be the same form in all media under investigation. Altering the sampling time of the received signal to account for this broadening is a part of the "tuning" of the device. The received signal should be a combination of translates of a single wavelet, the strength of which is proportional to the expression $(Z_2 - Z_1)/(Z_2 + Z_1)$. If desired, this can be corrected for absorption due to nonzero μ. The algorithm is described below. The received signal is given by

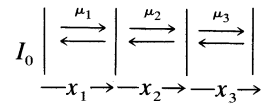

$$\begin{aligned} R = {} & I_0 e^{2\mu_1 x_1}(Z_2 - Z_1)/(Z_2 + Z_1) \\ & + I_0 e^{-2[\mu_1 x_1 + \mu_2 x_2]}(Z_3 - Z_2)/(Z_3 + Z_2) \\ & + I_0 e^{-2[\mu_1 x_1 + \mu_2 x_2 + \mu_3 x_3]}(Z_4 - Z_3)/(Z_4 + Z_3) \\ & + \cdots . \end{aligned} \tag{68}$$

The algorithm to correct for nonzero μ is described below.

When the received signal is transformed by a forward wavelet transform, the only **B** array terms that are nonzero are those for the levels j and $j - 1$. The **B** values give a direct map of the reflections.

The part (lower half) of the array **B** is a 1 by $N/2$ array that is converted (using this array and other values within **B** by a transformation which is described later into a 1 by N array called **R**). This is a direct map of the reflections and the magnitudes (if all absorption coefficients are assumed to be zero) are proportional to the $(Z_2 - Z_1)/(Z_2 + Z_1)$ terms of

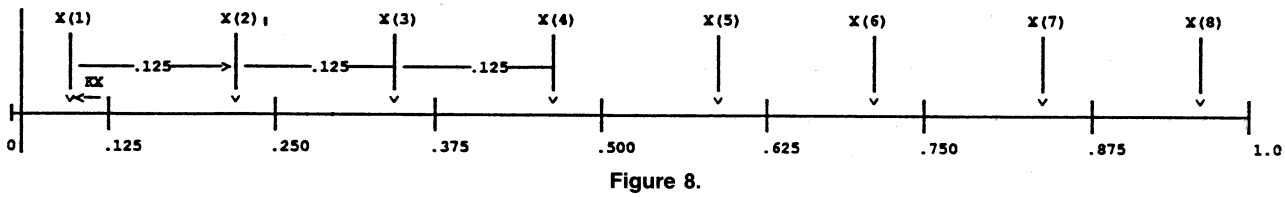

Figure 8.

Eq. (65). Consider now an array $\mathbf{Z}$ which is calculated from $\mathbf{R}$ by

$$(\mathbf{Z})_i = (\mathbf{Z})_{i-1} + (k \cdot i)\,\mathbf{R}_i\,. \tag{69}$$

This array represents data evenly spaced on the interval.

Assuming that the material being imaged is identical at the beginning of the scan ($i = 1$) to that at the end ($i = N$), then k is selected so that $\mathbf{Z}_N = \mathbf{Z}_1$. This compensates, approximately and efficiently, for nonzero absorption coefficients. Equation (67) converts the map of the reflection coefficients directly into a map of acoustical impedances (density times velocity of sound).

Clearly, $Z(x_{\max})$ should be $Z(x_{\min})$, else absorption has not been properly accounted for.

The imaging described herein will work for any degree of wavelet, i.e., for $M = 2, 4, \ldots$. The computational burden in performing the transform is directly proportional to the number of nonzero coefficients M; therefore it should be desirable to use the lowest-order wavelet possible. However, as a general rule, the higher the order of the wavelet, the easier it is to generate the time-reversed transmitted signal.

XIV. GENERATION OF THE ULTRASOUND WAVELET

Commercially available ultrasound transducers all possess resonances that makes it impossible to feed a voltage signal to the transducer and have the transducer produce a sound amplitude which is proportional to the applied voltage. However, linear system theory [4] offers a technique that allows us to present a signal to the transducer that is not what we want but is specifically designed to account for the precise manner in which the transducer will distort the signal so that, after the distortion, the desired signal shall be produced.

Consider the transducer to be a linear system with transfer function $G(s)$. That is given an input signal $f(t)$ with fourier transform $F(s)$, i.e., $F(s) = \mathrm{FT}(f(t))$, then the output signal $h(t)$ can be calculated because the fourier transform of $h(t) \equiv H(s)$ is given by $H(s) = F(s)\ G(s)$. So, $h(t)$ is the inverse fourier transform of $F(s)\ G(s)$.

The impulse response function of the system $g(t)$ is the inverse fourier transform of $g(s)$, i.e., $G(s) = \mathrm{FT}(g(t))$. Therefore the output signal $h(t)$ is the convolution of the impulse response function $g(t)$ with the input signal $f(t)$.

If we want the transducer to produce a defined $h(t)$, then the system should be offered a calculated input signal $f(t)$, rather than $h(t)$ itself (which would be given if the transducer were perfect, i.e., with an impulse response function which is an impulse). If this signal $f(t)$ is defined to be the convolution of $h(t)$ with $g^{-1}(t)$, then the transducer should produce $h(t)$ as its output. This is equivalent to adding another system in series with impulse response function $g^{-1}(t)$ to a system with the impulse response function $g(t)$. The time delay produced by this process is of no significance whatsoever.

Given a specific ultrasonic transducer, it is possible to generate a wavelet $w(t)$ with it by the following procedure:

1. Feed a sharp voltage spike to the transducer and dampen the response so that there are no zeros.
2. Measure the signal generated by the transducer. This is the impulse response of the transducer, $g(t)$.
3. Calculate $f(t)$, which is the inverse fourier transform of the product of $g^{-1}(t)$, and the fourier transform of the desired wavelet $w(t)$, which is $W(s)$.
4. Feed the signal $f(t) = \mathrm{FT}^{-1}(b^{-1}(t)\ \mathrm{FT}(w(t)))$ to the transducer. A good approximation of the wavelet $w(t)$ will be generated by the transducer.

XV. THE IMAGING PROCESS

The received ultrasound signals are transformed in accordance with the above transformation algorithms into a form representative of the acoustical impedances of the body materials. This information or data can be provided to the operator as numbers or it can be provided in a graphical form on a CRT or in hard copy. Usually, the signal representations will be provided to the operator in an image form such as from an oscilloscope or on a CRT, where the image corresponds to the body material interfaces, as are all well known in the art. Furthermore, the signals can be transformed into numerical values, graphs, or images of the density of the materials or the velocity of the sound through the body materials, again as are well known to those skilled in the art.

The invention described above was experimentally reduced to practice in the following manner. Wavelet generation was accomplished by a digital pulse generated by a computer command in a 33 MHz 80386 CPU equipped with a Cyrix EMC87 coprocessor. This CPU was connected to a SCI Wavelet Generator/Receiver Circuit Card that sent the signal to a Panametrics 500PR Pulse Receiver, connected in turn to a Panametrics 2.5 MHz V305SU F = 3.0″ ultrasonic transducer. The same transducer was used for sending and receiving. The signal was passed to the SCI Wavelet Generator/Receiver Circuit Card that stored the data in 8-bit evenly spaced points starting at the same time that a command was issued to transmit the $\mathbf{L}^{\mathbf{M}}$ wavelet.

An SCI MRI Coupler Card in the computer's CPU asked for the full transfer of the received data to RAM. The CPU then performed the single wavelet correction calculation, and a forward wavelet transformation on selected parts of the data; thereby the data of a single scan line was obtained which were the reflection coefficients. The reflection coefficients were then integrated to produce a map of acoustical impedances (density times velocity of sound) of the body materials. The transducer was physically moved to produce another scan line, with the set of obtained scan lines producing a rectangular image that was viewed directly as reflection coefficients or integrated to produce a map of acoustical impedances.

To illustrate the benefits of using this device to produce images of a quality better than that of the prior methods, an ultrasound device was used to generate a signal which is transmitted into a tomato in a container of water. This process (of obtaining a single scan line) is repeated 256 times by displacing the transducer by a small distance, yet keeping the focussed beam parallel to the previous one. Care is taken to assure that all scan lines are obtained in a single plane. From the received signal alone which is obtained by these conventional techniques, the internal structure of the tomato cannot be determined accurately by visual inspection of the set of signals.

Consider a single scan line. The reflection ultrasound signal can be calculated from the acoustical impedances by use of Eq. (68). Here all of the absorption coefficients can be taken

to have the value of $\mu_i = 0$. For the purposes of this example, the impedance is defined to be proportional to the measured (optical) density. This single line is shown in the plot labeled Z in Fig. 9. From the signal Z, the received ultrasound signal is calculated by well known techniques which are given by Eqs. (68) and (69) and is displayed in Fig. 9 by the plot labeled F. The wavelet transformation was applied to this function F and the resulting B array plot is shown. From the B array, above, using the techniques described herein, a calculated impedance is obtained and shown as the plot labeled V. Excellent agreement between Z and V can be observed.

The above procedure was carried out on all 256 scan lines of the image. The image on the left side of Fig. 10 is the calculated ultrasound signal, consisting of 256 individual scan lines. The image on the right shown in Fig. 10 is the results of performing the wavelet transformation reconstruction algorithm described herein on the data given on the left-hand image. The image of the ultrasound signal shown on the right is slightly superior to that obtained experimentally as complete correction for absorption has been made. Nevertheless, the image on the right-hand side is calculated entirely from the image on the left. No other data are employed in this

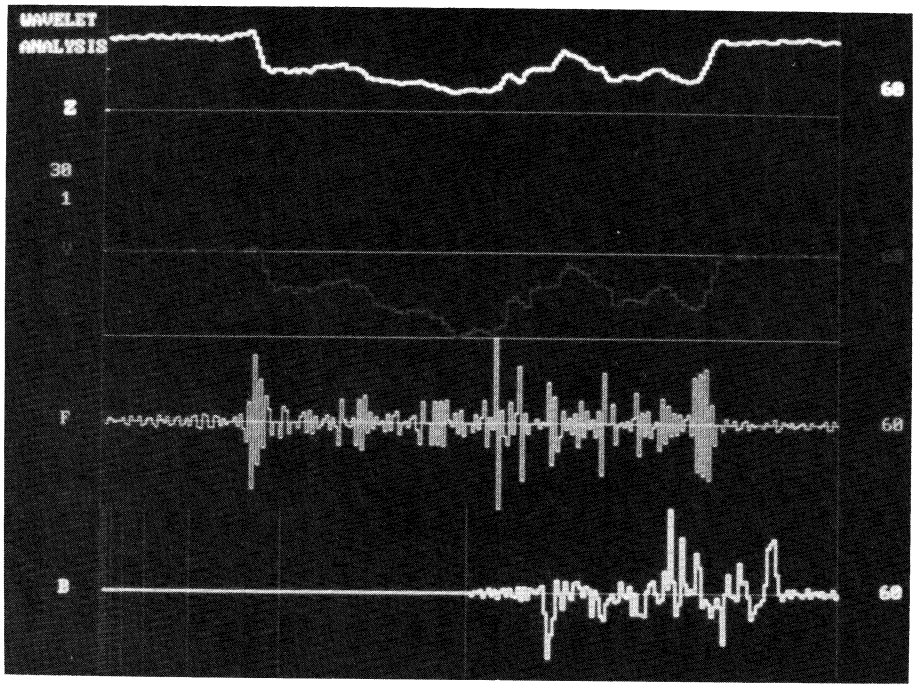

Figure 9. The plots of the calculated values of the received ultrasound signal F, the value of the B array obtained by applying the wavelet transformation on B and the calculated value of the impedance V.

Figure 10. The image on the left is the calculated ultrasound signal taken in a plane through the center of a tomato in a container of water. The image on the right is the result of performing the wavelet transformation reconstruction algorithm described herein on each of the scan lines of the image on the left.

calculation, so no claim is made that there is more *information* in the right-hand image than in the conventional image on the left. Yet it is felt that this mathematical transformation yields superior results because it offers the data in a form which makes it more meaningful to a human observer.

It should be noted that the *absolute* values of the impedances are not calculated, only the relative values. Therefore the absolute magnitude and gradient have been chosen by the author. A small amount of signal conditioning was performed. Two consecutive samples were adjusted to have identical values to prevent the reconstruction algorithm from generating nonzero occupation numbers for lower sequency wavelets. This restriction will be removed in the next paper of this series.

The process described above can be refined into a practical, portable, inexpensive, real time, noninvasive imaging device.

REFERENCES

1. J. Krautkramer and H. Krautkramer, *Ultrasonic Testing of Materials*, 4th ed., translated by J.D. Hislop (Springer-Verlag, Berlin/Heidelberg, 1990), pp. 16ff.
2. F. Harmuth Henning, *Transmission of Information by Orthogonal Functions* (Springer-Verlag, New York/Heidelberg/Berlin, 1970), pp. 49–50.
3. G. Strang, *SIAM Rev.* **31**, 614–627 (1989).
4. K. C. R. Castleman, *Digital Image Processing*, Signal Processing Series (Prentice-Hall, Englewood Cliffs, NJ, 1979).